Microsc. Microanal. 19, 1511–1522, 2013
doi:10.1017/S1431927613013226

Microscopy AND Microanalysis

Three-Dimensional Morphological and Mineralogical Characterization of Testate Amebae

Eric Armynot du Châtelet,[1,*] Catherine Noiriel,[2] and Maxence Delaine[1]

[1]*Université de Lille I, CNRS, Laboratoire Géosystèmes, 59655 Villeneuve d'Ascq, France*
[2]*Géosciences Environnement Toulouse (GET), Observatoire Midi-Pyrénées, Université Paul Sabatier, CNRS, IRD, 31400 Toulouse, France*

Abstract: Testate amebae are unicellular shelled protozoa commonly used as indicators in ecological and paleoecological studies. We explored the potential application of three-dimensional (3D) X-ray micro-tomography used in addition to 2D techniques (environmental scanning electron microscopy, electron probe micro-analysis, and cathodoluminescence) for detailed characterization of agglutinated shells of protozoa. We analyzed four specimens of the aquatic testate ameba *Difflugia oblonga* (Arcellinida), to test whether size distribution and mineral composition of shell grains diverged from sediment size distribution and mineralogical composition. From the 3D images, the geometry of the specimens (size and mass) and of the individual grains forming the specimen (grain size distribution and volume) were calculated. Based on combined chemical, mineralogical, and morphological analyses we show that *D. oblonga* is able to selectively pick up the small size fraction of the sediment with a preference for low-density silicates close to quartz density (~2.65). The maximum size of the grains matches the size of the pseudostome (shell aperture), suggesting the existence of a physical limit to grain size used for building the shell. This study illustrates the potential of this combined approach to characterize agglutinated shells of protozoa. This data can be useful for detailed morphological studies with applications in taxonomy and ecology.

Key words: testate amebae, 3D morphology, X-ray micro-tomography, cathodoluminescence, electron microprobe analysis, environmental scanning electron microscope

Introduction

Testate amebae are a group of ubiquitous unicellular shelled protozoa living in various environments like peatlands, rivers, lakes, or brackish-water settings (Charman, 2001). Their shell is composed of an inner organic (proteinaceous) matrix, which can be either secreted by the species or agglutinated, i.e., composed of extraneous mineral grains (xenosome). Testate amebae are considered as model organisms in ecology and paleoecology studies (Scott et al., 2001), and are used as bioindicators of environmental stress or pollution in both aquatic and terrestrial environments (Reinhardt et al., 1998; Patterson & Kumar, 2000). However, environmental factors that govern species distribution are still imperfectly known, so the interpretation of microfossil data remains equivocal. One bias may stem from the ecological conditions prevailing during the test construction. Indeed, many factors control testate amebae abundance and assemblage types, including nutrition, dissolved oxygen conditions, pH, salinity, substrate, or temperature (Gilbert et al., 2000; Scott et al., 2001). Two largely unexplored factors are sediment grain size and mineralogical composition.

Agglutinated testate amebae like *Difflugia* spp. select grains of different shape and size to form their three-dimensional (3D) test. As a consequence, the nature of the agglutinated tests may depend on their sedimentological environment, which can introduce some constraints and modifications in the structure of assemblages. For instance, some species are known to select the grains from the sediment (e.g., Eckert & McGee-Russell, 1974), and as a consequence, the texture of agglutinated tests can be highly variable (Armynot du Châtelet et al., 2010). Therefore, it is important to be able to identify the relationship between the grains forming the test and the sediment composition. A previous study has shown that the sediment grain size is a limiting factor for test construction, unlike the mineral composition (Armynot du Châtelet et al., 2010). However, a measurement bias was introduced due to the fact that the grains were analyzed only in 2D, from cross-sections. Advances in nondestructive 3D imaging techniques, such as X-ray micro-tomography (XMT), now allow for a full investigation of the 3D structure of the specimens. The technique is noninvasive and nondestructive, and can be used complementary to 2D analyses devoted to chemical and mineralogical characterization of the grains forming the test.

The aim of this study is to explore the potential of XMT for the study of testate ameba morphology. 3D investigation of the morphology of *Difflugia oblonga* involves: (1) a complete chemical and mineralogical characterization of tests using micro probe analysis, environmental scanning electron microscopy equipped with energy-dispersive spectroscopy (ESEM-EDS), and cathodoluminescence (CL) Technics, together with (2) a full characterization of the 3D geometry of the agglutinated tests as well as all of their forming grains using XMT. We compare the characteristics

Received February 25, 2013; accepted July 15, 2013
*Corresponding author. E-mail: eric.armynot@univ-lille1.fr

of grains used for shell construction with grains from sediments from the same sampling location.

Materials and Methods

Study Area and Sediment Sample

A volume of 50 cm^3 of sediment was sampled in the Clairmarais ponds (50°46′59.40″N, 2°18′22.91″E, Pas-de-Calais, France). The ponds are located ~30 km from the sea in the Flemish coastal plain, and correspond to Holocene infilling of lower terrains as a result of the rising sea level (Gandouin et al., 2005). Both the plain and ponds are connected to the North Sea through the Aa River. The available rocks around the sampling area are mostly clay, marl, and chalk (Waterlot, 1968).

Half of the sediment volume was used for testate amebae collection, and the other for sediment analysis. Two specimens of testate amebae from the species *D. oblonga* were sampled for XMT analysis (specimens 1 and 2) and two others for ESEM-EDX and microprobe analysis (specimens 3 and 4).

Sediment Characterization

Grain-size distribution of the sediment was determined using the principle of diffraction of a monochromatic laser beam on suspended grains (Malvern Mastersizer 2000, red He-Ne laser, 632 and 466 nm wavelengths). The method, a detailed description of which can be found in Trentesaux et al. (2001), is based on near-forward scattering of a laser beam by grains in suspension (Loizeau et al., 1994). Measurements were done in the range 0.02–2,000 μm (with an obscuration comprised between 10 and 20%). The main mode and descriptive parameters of the grains were determined along with grain-size distribution. Sediment distribution was divided in six fractions: clay (<2 μm), fine silt (2–10 μm), sortable silt (10–63 μm, McCave et al., 1995), fine and very fine sand (63–250 μm), medium sand (250–500 μm), and coarse and very coarse sand (>500 μm). Sorting and skewness were also used as descriptive parameters.

Mineral diversity of the grains composing the sediment was determined using punctual ESEM-EDS analyses on individualized grains.

Chemical Characterization of the Agglutinated Grains

ESEM Equipped with EDS

As a preliminary measurement, chemical composition of the minerals agglutinated within the test walls of *D. oblonga* specimens 3 and 4 was determined on polished C-coated sections by means of elemental chemical mapping using ESEM equipped with an EDS deviceto detect Al, Ca, Fe, Si, K, Mg, Na in the tests under low-vacuum conditions with a 20 kV beam. Chemically coded color imaging helped to separate the different grains according to their chemical composition, while conventional backscattered electron (BSE)-imaging helped to localize heavy element-rich grains due to their stronger reflectivity, even if the method was useless for distinguishing between orthoclase and plagioclase feldspars.

Electron Probe Micro-Analysis

In addition, chemical measurements of the minerals forming the two specimens already characterized with ESEM-EDS (i.e., specimens 3 and 4) were analyzed using an electron probe micro-analyzer (EPMA) (Cameca SX100, Madison, WI, USA) equipped with four wavelength-dispersive spectrometers. X-ray profiles and quantification were carried out at 15 kV and 20 nA.

CL

Grayscale SEM-CL images were collected from two polished and C-coated sections of *D. oblonga* specimens 3 and 4, on a Quanta 200 SEM (FEI Company, Hillsboro, OR, USA; www.vsg3d.com/avizo/) equipped with a CL Centaurus sensor using an accelerating voltage of 30 kV. This technique can provide essential information on growth fabrics, diagenetic textures, and mineral zonation as luminescence of natural minerals arises from defects in the crystal structure or impurities in the crystal lattice, resulting in different colors and intensities. These images allow for evaluating both degree of alteration and zonation of the minerals. Images were collected on the same specimens analyzed with ESEM-EDS and EPMA. The samples had to be slightly polished between analyses. As a consequence, the sections were slightly different.

3D Geometry with XMT

The 3D geometry of two different specimens of *D. oblonga* (specimens 1 and 2) was characterized by XMT at the Swiss Light Source, Beamline TOMCAT (SLS, Villigen, Switzerland). The XMT method is based on 3D reconstruction from a thousand 2D radiographs of the X-ray attenuation properties of the various materials forming the specimens. At a given beam energy, absorption of X-rays is a function of several physical parameters, mainly the local density and the atomic number of the material being traversed. As air (background), oxides, and silicate minerals in the rock have different elemental compositions, their attenuation properties are different. Therefore, they can be differentiated on the 3D images. It is worth noting that organic matter has too low of an attenuation coefficient compared to minerals to be distinguished on the images. As a result, organic vesicles (e.g., Ogden, 1988) cannot be interpreted as xenosome grains.

Specimens were scanned with an X-ray beam energy of 20 keV using a double crystal multilayer monochromator. The optical system used in the experiment provided a spatial resolution of 0.37 μm (pixel size). A data set containing the two specimens stuck on a tip was collected. Acquisition was performed using the phase contrast mode in order to enhance the contrast at edges between minerals and the background (Salvo et al., 2003). The radiographs were filtered before reconstruction to eliminate the random noise

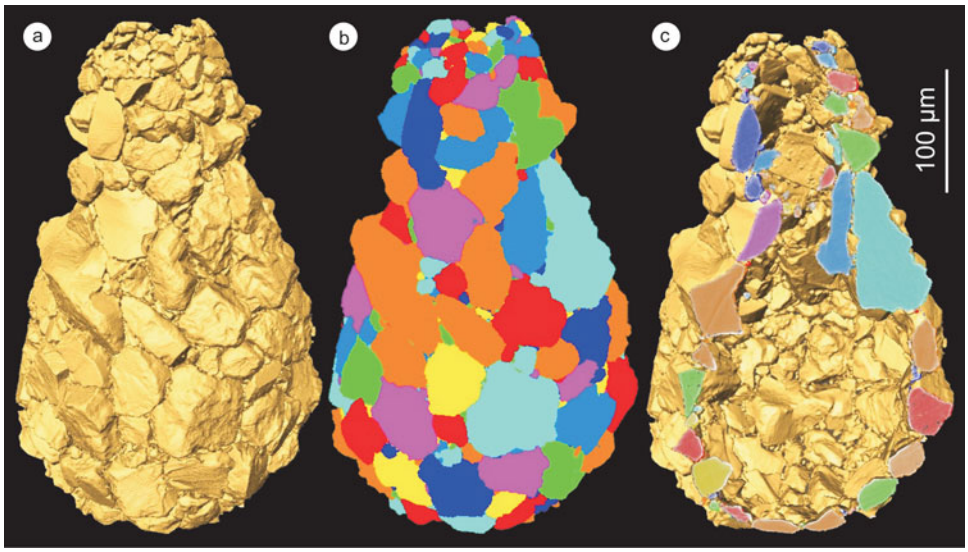

Figure 1. **a**: Three-dimensional rendering view of the test of *Difflugia oblonga* (specimen 1) obtained after the segmentation procedure and (**b**) labeling of the grains. **c**: Truncated view of the specimen showing the internal structure. The scale bar is applied for the cross-section shown in (**c**).

due to high-energy diffracted photons and the ring artifacts (Bernard & Chirazi, 2006). Volume reconstruction was carried out using direct Fourier inversion, through the use of a filtered back-projection algorithm (Herman, 1980). The reconstruction provided a 3D image of the X-ray absorption by the different materials in the sample. The volume (V_{256}) of the initial data set was around 2,000 × 2,000 × 700 voxels. A voxel (M) is defined as a pixel cubed and is represented as a volume of 0.37 × 0.37 × 0.37 μm^3.

Image processing was achieved using Avizo® software (FEI Visualization Sciences Group, Burlington, MA, USA). By using an appropriate image processing procedure it was possible to remove the background, separate the two specimens, identify the different materials (e.g., air from oxides and silicate minerals), and accurately quantify parameters characterizing the specimen geometry, i.e., grain size distribution (surface, volume) and sphericity. Sphericity ψ [equation (1)] tends to 1 as grain shape becomes more spherical:

$$\psi = \frac{\pi^{1/3}(6 \times V)^{2/3}}{S}, \tag{1}$$

where V is the volume of the grain and S its surface.

The procedure was as follows. First, the original 32-bit accuracy grayscale data set was converted into an 8-bit grayscale data set (i.e., 256 gray levels) and the noise was reduced by running a 3D median filter. Then, the two specimens in the image were separated and registered on an orthonormal basis (x, y, z). Second, the background was removed. To do this, the images were segmented; i.e., the voxels belonging to the background were distinguished from those belonging to the specimens. Despite the fact that data were noisy and presented phase contrast, a segmentation technique based on a threshold value was successfully applied to separate the background from the different materials forming the specimens (Gonzales & Woods, 1992), after some manual corrections of the star artifacts which could have bothered the segmentation procedure. A threshold value of 120 for segmentation was chosen by visual inspection of the gray-level histogram and of the segmented volume by comparison with the grayscale one. At the end of the procedure, the background was set to 0 and the solid phase (grains) to 1:

$$V_{\text{seg}}(x, y, z) \begin{cases} 0 & M(x, y, z) \in \text{background} \\ 1 & M(x, y, z) \in \text{grain.} \end{cases} \tag{2}$$

For a better visualization, the initial volume was combined with the segmented volume [equation (3)], so that the background was set to 0 as the grains kept their original gray value. At this stage, it was still possible to qualitatively distinguish between quartz and feldspar (despite both silicate minerals having close densities), the last being microporous due to alteration:

$$V_{256} \otimes V_{\text{seg}}. \tag{3}$$

As the different grains forming the specimens are more or less agglomerated, an algorithm based on watershed separation was then applied. By combining fast watershed, distance, and numerical reconstruction algorithms, it was possible to isolate each grain of the specimen. Unwanted separation that occurred for some nonconvex shape grains was corrected manually by comparison with the gray-level volume. Then, the different grains were labelled (Fig. 1), and their shape descriptors were computed.

Surface, volume, and sphericity were used as descriptive parameters of the grains. Significant differences in mean values of grain volume calculated every 25 μm were detected by one-way analysis of variance (ANOVA). Data normality and homogeneity of variances were previously checked. When these ANOVA assumptions were violated, a log transformation was applied to data prior to analysis. Tukey's 'Honest Significant Difference' (Tukey's HSD) *post hoc* comparison of means was used to detect differences among slices. In all cases, significance level adopted was 95% ($\alpha = 0.05$). Calculations were performed using *R* package *base*.

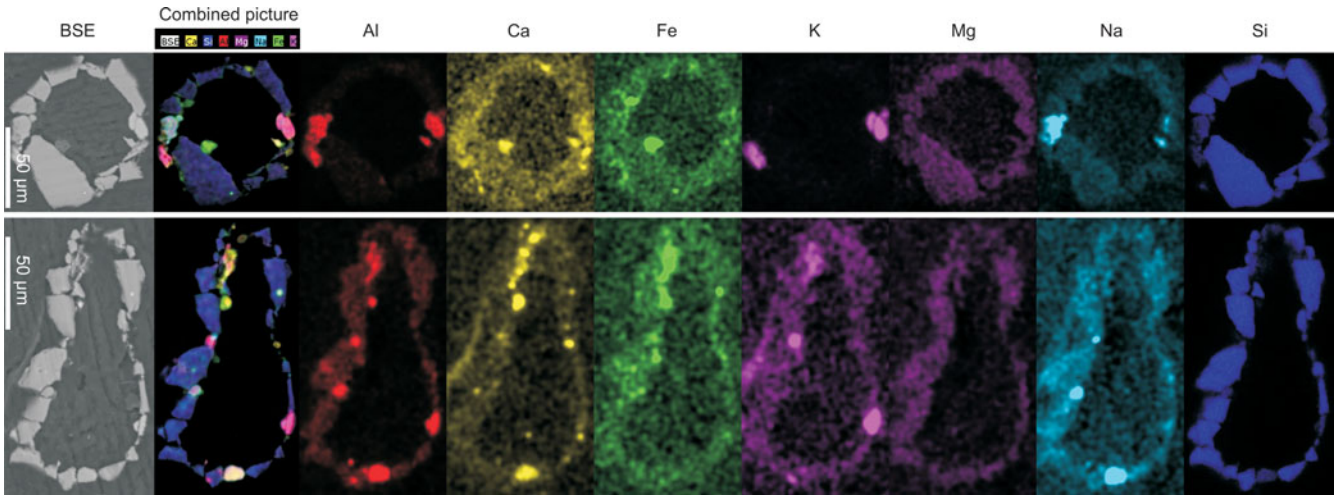

Figure 2. ESEM-EDX analysis of specimens 3 and 4. Combined picture is a superimposition of the map of the detected element (Al, Ca, Fe, K, Mg, Na, Si). ESEM-EDX, environmental scanning electron microscopy-energy-dispersive spectroscopy, BSE, backscattered electron.

Mass of the two specimens was estimated from their volume and grain density, assuming that (1) the proportion of the different test-forming minerals determined by image analysis on 2D thin sections is still valid in 3D, and (2) the mineral distribution in the test determined for specimens 3 and 4 is similar for every specimen living in the same environment (Armynot du Châtelet et al., 2010).

Results

Chemical Composition of the Tests

ESEM-EDS chemical analysis of specimens 3 and 4 indicated grains differentially rich in Ca, Fe, K, Mg, K, Na, and Si (Fig. 2). Twenty of the 22 microprobe analyses allowed identification of six silicate minerals according to their chemical composition: albite, orthoclase and oligoclase (feldspars), quartz, epidote (Armbruster et al., 2006), and amphibole (Hawthorne & Oberti, 2007). Two analyses also pointed out two nonpure quartz grains probably associated with organic matter (Fig. 3, Table 1). The mineral mapping interpretation is reported in Figures 3e and 3f. In addition, very small bright grains agglutinated on the external part of the test of specimens 1 and 2 are interpreted as Fe–Ti–oxides (Figs. 4g, 4j).

From CL observations, grains were shown to be nearly homogenous without any zonation growths (Fig. 5). The grains forming the two analyzed specimens are both perfect crystals and crystals including imperfections. The crystal imperfections (luminescent grains) are observed in quartz and orthoclase in the specimen observed in the coronal plane (Fig. 5a) and albite and orthoclase in the specimen observed in the transverse plane (Fig. 5b).

3D Morphology of the Skeleton

All grains forming the skeleton were analyzed after the segmentation and labelling procedures (Figs. 1b, 1c). The main characteristics of the grains forming the two specimens are presented in Table 2. The two specimens are large enough to allow the analysis of their individual grains. Specimens 1 and 2 are 367 and 393 μm long, respectively. The shell is roughly circular for the first specimen (minor axis/major axis = 1.05) and compressed for the second specimen (minor axis/major axis = 1.45). For both specimens, the pseudostome is perfectly circular (minor axis/major axis = 1).

The relative abundance of the minerals in the two specimens analyzed in thin section was estimated (Table 3). From the knowledge of the density of each of these minerals (Table 3) and the total number of grains (Table 2), the mass of the two specimens was estimated to be 7.44 and 6.89 μg, respectively.

On sagittal slices (Fig. 4), grains are oriented preferentially along their long axis, wrapping round the cell of the specimens. Distribution of the grain size along the *Z*-axis (sagittal and transverse view of Fig. 4) shows two different trends (Fig. 6): close to the pseudostome (aperture), all of the grains are small (Figs. 6a, 6b) unlike the rest of the test. As a consequence, the ratio between the number of grains and the perimeter of the test is higher in this area (Figs. 6c, 6d). Small grains are also found elsewhere in the test, where they fit in between bigger grains.

For specimen 1, all grain volumes sliced by class of 25 μm along the *Z*-axis could be considered homogenous ($p > 0.05$ for ANOVA results in Table 4 and Tukey's HSD *post hoc* in Supplementary Material 1) except grain volumes from 0–25 to 125–150 μm. These two classes of grains correspond to the pseudostome and the beginning of the transition between the neck and the main body.

For specimen 2, the mean grain volume cannot be considered homogenous throughout the specimen ($p < 0.05$ for ANOVA in Table 4). Nevertheless, Tukey's HSD investigation provides a probability of $p > 0.05$ for slices compared in twos (Supplementary Material 2). Hence, grain distribution could be considered homogenous through most of the specimen.

Supplementary Material

To view Supplementary Materials 1 and 2 for this article, please visit http://dx.doi.org/10.1017/S1431927613013226.

None of the measured grains are spherical (Fig. 7). For the first specimen (Fig. 7a), the mean sphericity along the test is nonhomogenous (Table 4, $p < 0.05$). Tukey's HSD analysis shows that the nonglobal nonhomogeneity of the mean is mainly due to the 25–50 μm class, which is not comparable to the following classes: 0–25, 100–125, 125–150, 150–175, 175–200, and 200–225 μm (Supplementary Material 1). This class contains some elongated grains with a very small sphericity. For the second specimen (Fig. 7b), the mean sphericity is also nonhomogenous (Table 4, $p < 0.05$). Tukey's HSD analysis shows numerous differences between the sphericity of the different slices (Supplementary Material 2).

Comparison between the Mineral Composition of the Sediment and the Mineral Composition of the Test

The sediment of the Clairmarais ponds is mainly composed of calcite grains (67.5%), associated with quartz (25.3%) and feldspar (6.0%) grains. The sediment also contains rare altered amphiboles (<1%) and epidotes (only one grain was observed, <1%). Many oxide grains are observed as well as small framboiidal pyrites (<5 μm; <1%). Except for the dominant calcite, all other minerals are agglutinated on the specimens of testate amebae.

Comparison between Grain Size of the Sediment and the Grain Size of the Test

The sediment grain size of the Clairmarais ponds corresponds mainly to sortable silt and fine to medium sand (Fig. 8). The sediment mode is 151.2 μm. The mean size is 243 μm and the median (D_{50}) is 91 μm. D_{90}–D_{10} is equal to 393 μm. Sediments are badly sorted (1.91), but the skewness indicates that the distribution is close to symmetrical (−0.04).

The grain sizes used by the two specimens of *D. oblonga* to construct their test are very different compared to the main sediment (Fig. 9). Only the smallest grain fraction is selected. The grain distributions of the two specimens of *D. oblonga* are not comparable in terms of mean volume (Welch Two Sample *t*-test: $t = 6.9159$, df = 871.997, $p = 8.986 \times 10^{-12}$) and the distributions follow different distribution laws (two-sample Kolmogorov–Smirnov test: $D = 0.1774$, $p = 2.05 \times 10^{-10}$). Nevertheless, each specimen is capable of selecting its own grains among the range of the small size sediment grains. Interestingly, the maximum size of observable grain agglutinated on the test corresponds to the maximum volume-equivalent size of the pseudostome of the test (Fig. 9 lines α and β).

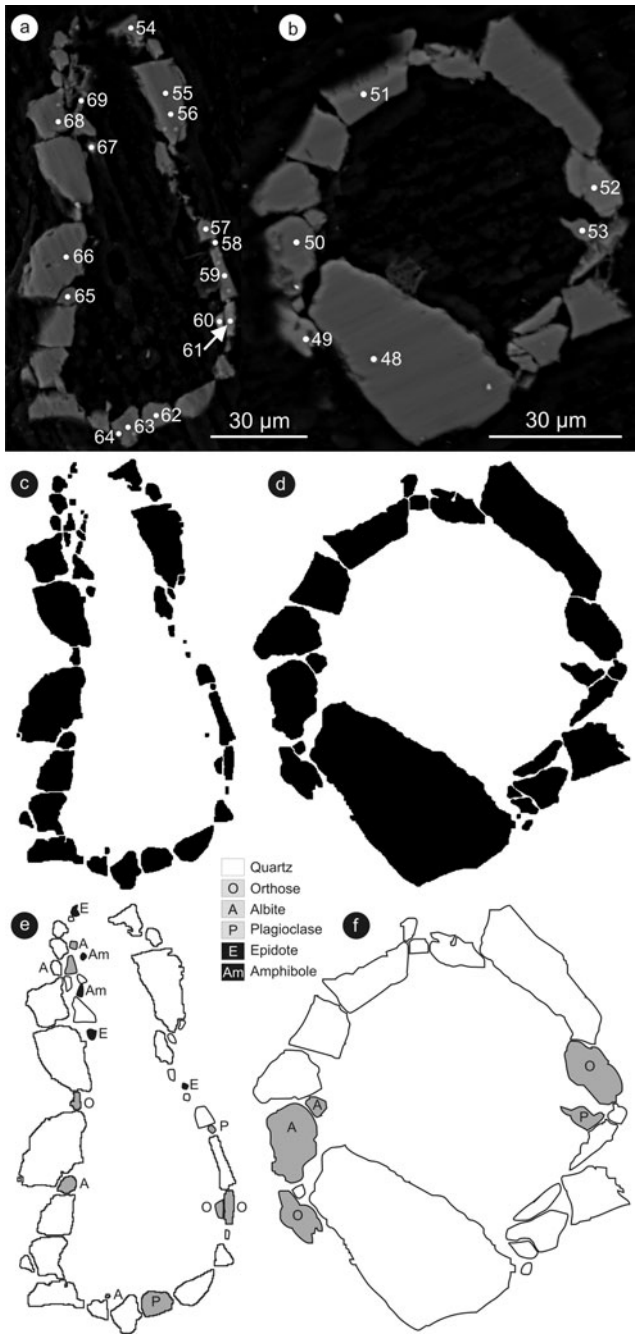

Figure 3. a, c, e: Sagittal views of specimen 3. **b, d, f**: Transverse views of specimen 4. **a, b**: Position of points analyzed with microprobe positioned on a mixed image (BSE and SE). **c, d**: BSE image after gray-level threshold adjustment (8-bit) and watershed treatment. **e, f**: Map of minerals interpreted after ESEM-EDS analyses (Fig. 2). ESEM-EDX, environmental scanning electron microscopy energy-dispersive spectroscopy, BSE, backscattered electron, SE, secondary electron.

Discussion

Test Composition Versus Nature and Origin of the Mineral Fluxes

In this study, several minerals were found in the specimens tests. The nature and potential origin of xenogenous grains

Table 1. Microprobe Analysis Results with Determination of Minerals.*

Number of Analysis	1	2	3	4	5	6	7	8	9	10	11
SiO_2	95.86	62.33	64.45	94.64	67.29	64.65	93.60	96.75	92.87	93.13	61.39
TiO_2	0.01	0.01	−0.02	−0.01	0.02	−0.01	0.00	0.00	−0.01	0.00	0.05
Al_2O_3	0.01	19.66	22.88	0.00	19.37	24.30	0.03	0.00	0.03	0.00	16.69
FeO	0.00	0.04	0.01	−0.03	0.07	0.07	0.02	0.02	0.00	−0.02	0.32
MnO	0.00	0.03	0.02	−0.01	0.01	−0.02	−0.01	0.02	−0.01	−0.01	0.02
MgO	−0.01	0.02	0.00	0.00	0.00	0.00	0.02	−0.01	0.01	−0.01	0.15
CaO	0.01	−0.05	0.54	0.01	−0.05	3.61	0.11	0.01	0.03	0.00	0.37
Na_2O	0.00	0.30	10.17	0.02	0.54	9.35	0.02	0.01	−0.01	0.02	5.47
K_2O	0.00	16.58	0.06	0.00	10.31	0.15	0.02	0.02	0.03	0.02	0.31
NiO	0.00	−0.01	−0.01	0.00	0.01	0.02	0.00	−0.02	0.04	−0.02	−0.02
Oxygens =	2	8	8	2	8	8	2	2	2	2	8
Si	1.00	2.93	2.87	1.00	3.06	2.79	1.00	1.00	1.00	1.00	3.09
Al	0.00	1.09	1.20	0.00	1.04	1.24	0.00	0.00	0.00	0.00	0.99
Ti	0.00	0.00	0.00	0.00	0.00	0.00	0.00	0.00	0.00	0.00	0.00
Fe	0.00	0.00	0.00	0.00	0.00	0.00	0.00	0.00	0.00	0.00	0.01
Mn	0.00	0.00	0.00	0.00	0.00	0.00	0.00	0.00	0.00	0.00	0.00
Mg	0.00	0.00	0.00	0.00	0.00	0.00	0.00	0.00	0.00	0.00	0.01
Zn	0.00	0.00	0.00	0.00	0.00	0.00	0.00	0.00	0.00	0.00	0.00
Ca	0.00	0.00	0.03	0.00	0.00	0.17	0.00	0.00	0.00	0.00	0.02
Na	0.00	0.03	0.88	0.00	0.05	0.78	0.00	0.00	0.00	0.00	0.53
K	0.00	0.99	0.00	0.00	0.60	0.01	0.00	0.00	0.00	0.00	0.02
Ni	0.00	0.00	0.00	0.00	0.00	0.00	0.00	0.00	0.00	0.00	0.00
Total of atoms	1.00	5.04	4.97	1.00	4.74	4.99	1.00	1.00	1.00	1.00	4.69
Total weight	95.9	98.8	98.1	94.5	97.4	102.1	93.7	96.7	92.9	93.0	84.8
Name of the mineral	Quartz	Orthose	Albite	Quartz	Orthose	Feldspar (Plagioclase: Oligoclase)	Quartz	Quartz	Quartz	Quartz	Plagioclase

Number of Analysis	12	13	14	15	16	17	18	19	20	21	22
SiO_2	94.22	56.16	56.49	61.62	94.25	70.06	69.11	97.60	37.81	96.38	32.06
TiO_2	0.02	0.02	0.02	0.01	0.02	0.10	0.01	−0.01	0.02	0.01	0.24
Al_2O_3	0.04	16.54	17.80	23.95	0.08	17.74	20.78	0.01	25.55	0.08	15.26
FeO	0.00	0.01	−0.01	0.05	0.00	0.62	0.01	0.02	8.19	0.02	6.36
MnO	−0.02	0.02	0.01	0.02	−0.01	0.00	−0.01	−0.01	0.13	0.04	0.06
MgO	0.00	0.00	0.01	0.00	0.00	0.33	0.01	0.00	0.04	0.01	1.64
CaO	0.00	0.20	0.04	4.74	0.01	0.10	0.22	0.03	17.45	0.06	3.64
Na_2O	0.03	0.63	0.52	8.85	0.06	0.49	10.35	0.00	0.05	0.03	0.94
K_2O	0.06	12.61	12.48	0.11	0.01	2.32	0.07	0.02	0.04	0.04	2.89
NiO	0.00	−0.04	−0.03	−0.02	0.00	−0.04	0.01	0.02	0.01	−0.03	0.01
Oxygens =	2	8	8	8	2	2	8	2	12.5	2	23
Si	1.00	2.99	2.95	2.75	1.00	0.80	2.98	1.00	3.22	1.00	6.96
Al	0.00	1.04	1.10	1.26	0.00	0.24	1.06	0.00	2.57	0.00	3.91
Ti	0.00	0.00	0.00	0.00	0.00	0.00	0.00	0.00	0.00	0.00	0.04
Fe	0.00	0.00	0.00	0.00	0.00	0.01	0.00	0.00	0.58	0.00	1.16
Mn	0.00	0.00	0.00	0.00	0.00	0.00	0.00	0.00	0.01	0.00	0.01
Mg	0.00	0.00	0.00	0.00	0.00	0.01	0.00	0.00	0.01	0.00	0.53
Zn	0.00	0.00	0.00	0.00	0.00	0.00	0.00	0.00	0.00	0.00	0.00
Ca	0.00	0.01	0.00	0.23	0.00	0.00	0.01	0.00	1.59	0.00	0.85
Na	0.00	0.06	0.05	0.77	0.00	0.01	0.87	0.00	0.01	0.00	0.39
K	0.00	0.86	0.83	0.01	0.00	0.03	0.00	0.00	0.00	0.00	0.80
Ni	0.00	0.00	0.00	0.00	0.00	0.00	0.00	0.00	0.00	0.00	0.00
Total of atoms	1.00	4.95	4.94	5.01	1.00	1.10	4.92	1.00	8.00	1.00	14.65
Total weight	94.3	86.4	87.3	99.2	94.4	91.9	100.6	97.6	89.2	96.6	64.5
Name of the mineral	Quartz	Orthose	Orthose	Feldspar (Plagioclase: Oligoclase)	Quartz	Quartz	Albite	Quartz	Epidote	Quartz	Amphibole

*The labels correspond to the points displayed in Figure 2.

are highly diverse and variable. Early research work described quartz as the main mineral forming the test. Despite calcite being the most abundant mineral in the sediment, quartz is certainly dominant in the test because of its high stability and strength compared to most of the other minerals available in surface sediments. Armynot du Châtelet et al. (2010) described many other minerals, like chlorite, muscovite, Fe-oxide, microcline, albite, calcite, rutile, sericite-(Al), and sericite-(Fe, Mg, Si). In the present study, we observed six minerals within the test, the occurrence of

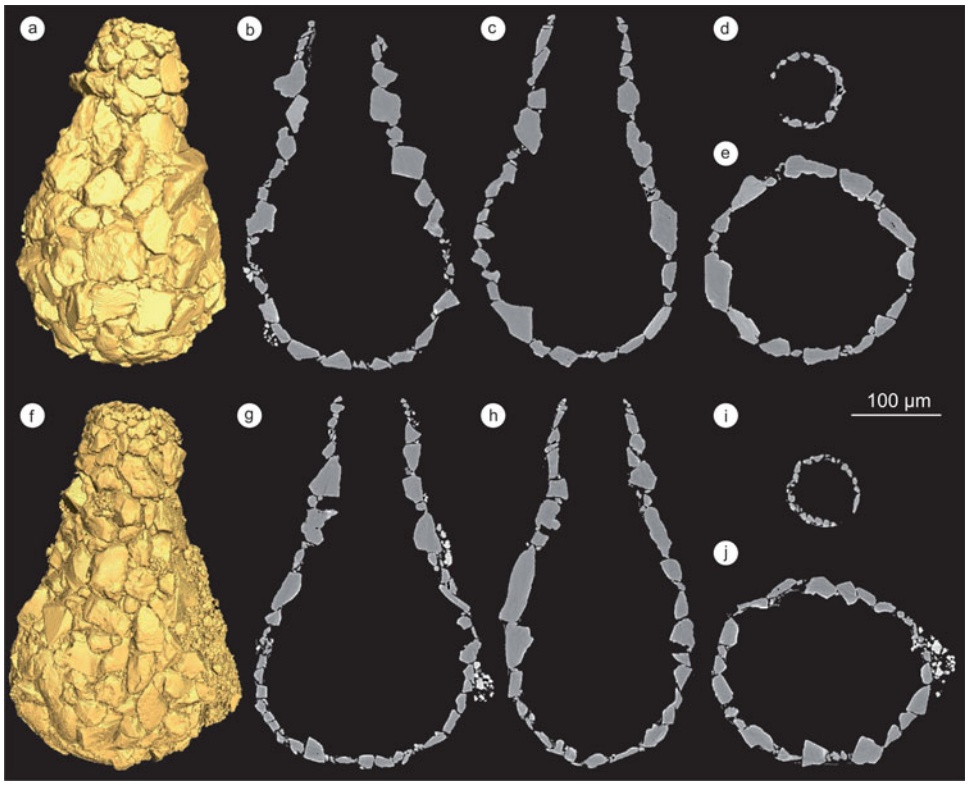

Figure 4. Different cross sections of the two specimen of *Difflugia oblonga* (**a, f**) obtained with X-ray micro-tomography after background removal: (**b, g**) sagittal view; (**c, h**) coronal view; (**d, i**) transverse view of the pseudostome; (**e, j**) coronal view of the largest part of the body.

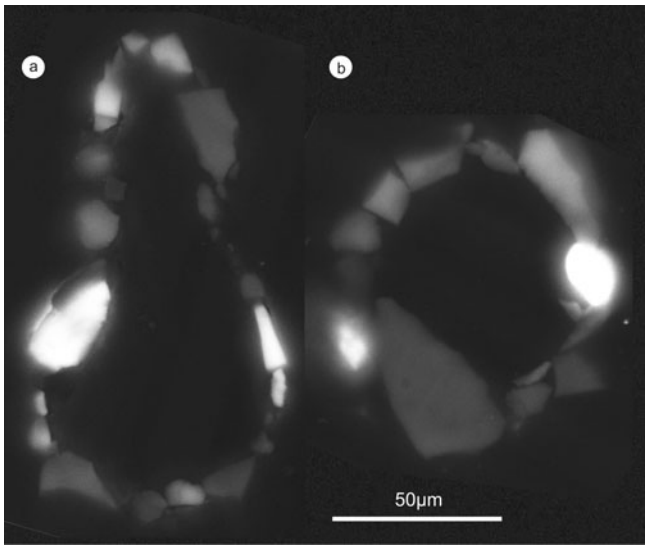

Figure 5. Cathodoluminescence analysis of specimens 3 and 4 of *Difflugia oblonga* cut following (**a**) a coronal plane and (**b**) a transverse plane.

which certainly depends on minerals available in the sediment. The minerals are probably primarily selected according to their size to fit on the cytoplasm (Eckert & McGee-Russell, 1974). However, despite the density of the grains being variable, from 2.55 (orthoclase) to 3.6 (amphiboles), the analysed specimens preferentially select grains of similar densities, probably to keep the test balanced. Moreover, it is worth noting that the grains of lowest density (i.e., orthoclase and quartz) are preferentially agglutinated. From this observation, quartz appears to be the best candidate because its density is very stable (2.65) compared to other minerals for which density differs according to their structure and alteration degree (Drever, 1985). The properties of quartz probably simplify the choice for selecting grains in order to construct an equilibrated test. Despite the fact that

Table 2. Main Characteristics of the Test and Their Grains of the Two Specimens (1 and 2) of *Difflugia oblonga*.

	Specimen 1	Specimen 2
Test characteristics		
Estimated mass (μg)	7.44	6.89
Height		
Internal (μm)	367	393
External (μm)	375	399
Pseudostome		
Major axis (μm)	70	66
Minor axis (μm)	70	66
Body		
Major axis (μm)	192	219
Minor axis (μm)	182	151
Grains characteristics		
Number of grains	514	1265
Volume (μm^3)		
Total	2,811,659.69	2,603,269.2
Mean	5,470.2	2,057.9
Min	10.7	9.0
Max	165,952.8	80,647.8
Surface (μm^2)		
Mean	5,470.2	2,057.9
Minimum	10.7	9.0
Maximum	165,952.8	80,647.8

Table 3. Surface Proportion of the Minerals Determined on the Sections of Specimens 3 and 4 and Mean Density of the Minerals.

	Theoretical (%)	Density
Quartz	87.40	2.65
Orthose	5.17	2.55
Albite	4.80	2.6
Plagioclase	2.06	2.6
Epidote	0.34	3.435
Amphibole	0.22	3.15

Table 4. Difference Investigation between the Volume of the Grains Grouped in Slices of 25 μm Thick Along the *Z*-Axis (Growth Axis).*

	Df	Sum Sq	Mean Sq	*F*-value	Pr(>*F*)
Specimen 1					
Volume	14	99.48	7.11	1.65	0.062
Sphericity	14	1.15	0.08	3.50	0.000
Specimen 2					
Volume	15	234.80	15.65	4.53	0.000
Sphericity	15	1.88	0.13	5.34	0.000

*Results of ANOVA are given as: df, sum Sq, mean Sq, as well as *F*-value and Pr(>*F*) are given. When *p*-values are >5% variance model should be accepted.

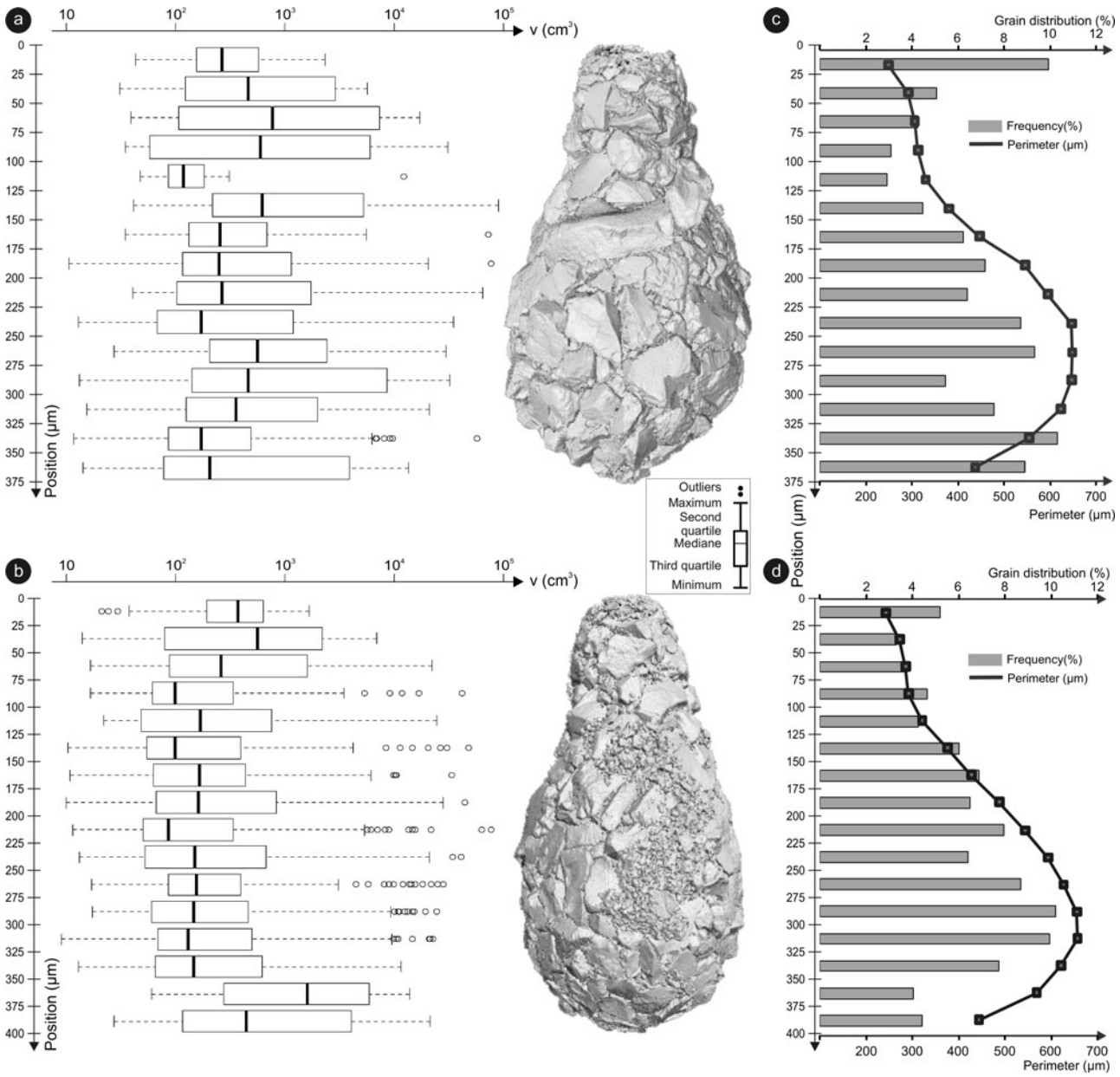

Figure 6. Grain volume distribution along specimens 1 and 2. Volumes are characterized with box and whisker plot every ~25 μm (**a, b**). On each of these classes, the ratio between the perimeter and the number of grains as well as the number of grains are given (**c, d**).

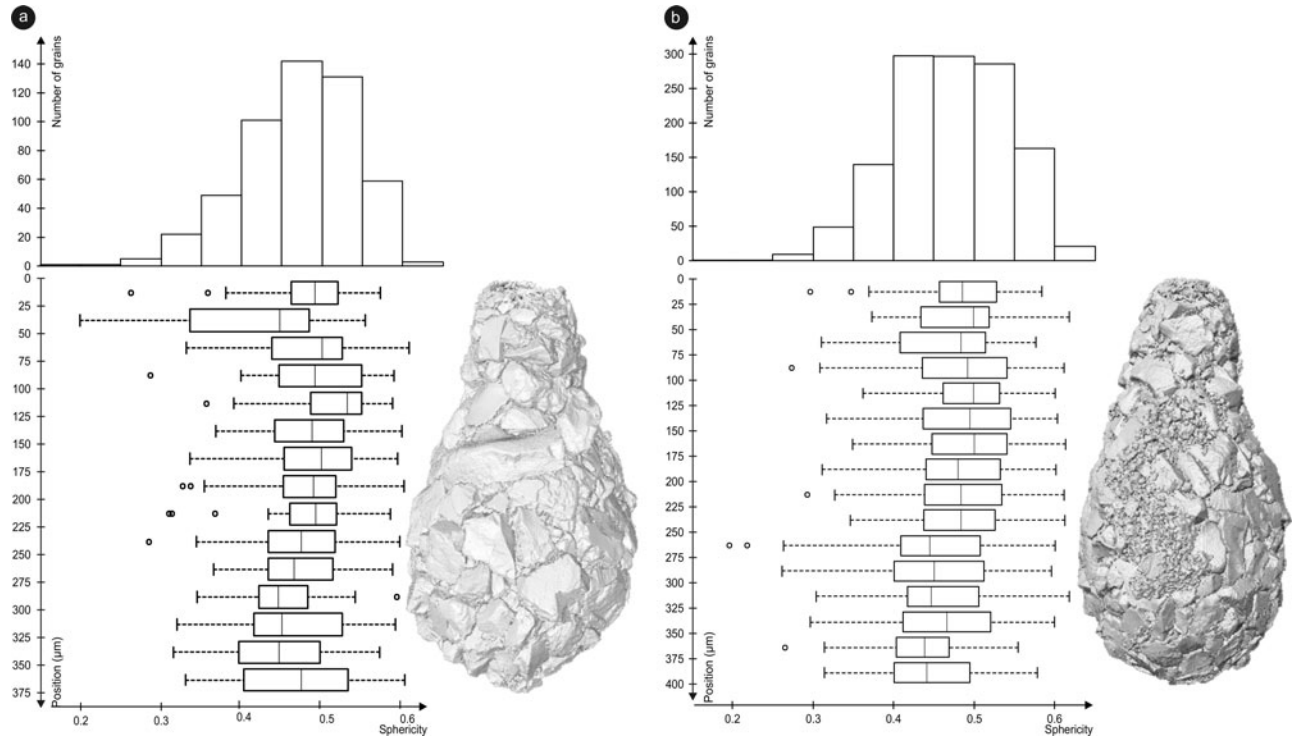

Figure 7. Sphericity distribution along the test of specimens 1 and 2. Volumes are characterized with boxes and whiskers every ~25 μm. The global sphericity distribution is shown in the histogram.

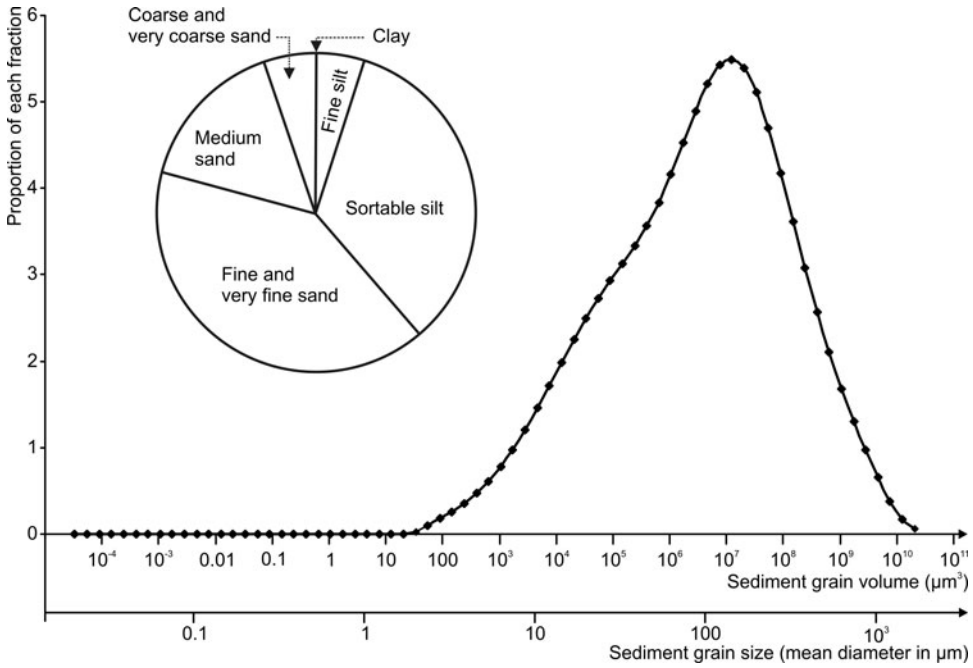

Figure 8. Sediment size distribution of the Clairmarais pond. The mean diameter of the grains is given as well as their estimated volume assuming a spherical shape.

calcite grains are numerous in the sediment, it is worth noting that they were not observed in the test. Calcite, which is shown to be often altered, does not present a well crystallized shape, and was probably avoided by testate amebae to construct their tests for that reason.

In addition, it is possible from the mineral distribution of the grains to trace their geological origin. This tracing could be accompanied by a modelling of the air fluxes for oligotrophic peat land deposits or river fluxes (mineral load) for minerotrophic peat lands or any other watershed connected ecosystem where testate amebae are living. The available rocks around the sampling area are mostly clay, marl, and chalk (Waterlot, 1968). Feldspar and quartz could be observed (in low abundance) essentially within the clay and hence could be inherited from these rocks. Nevertheless, amphiboles and epidotes have never been described in

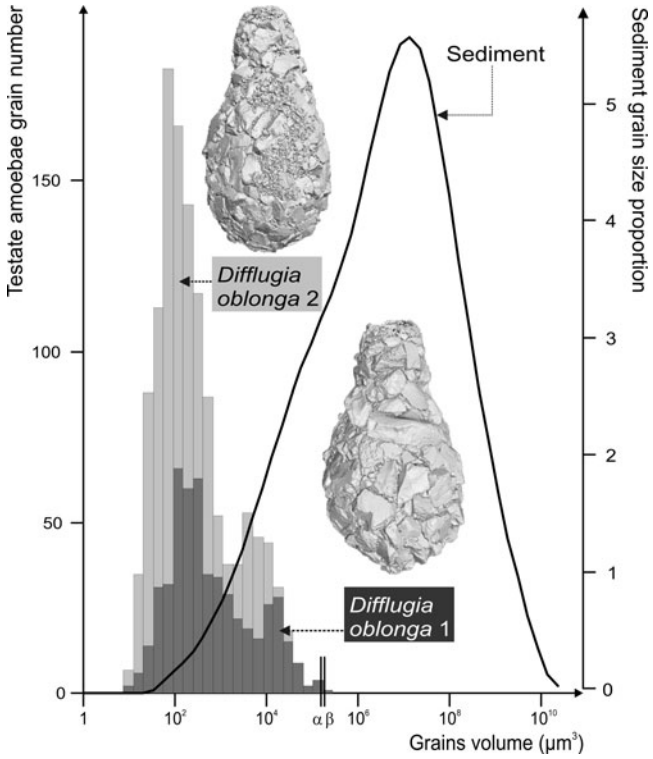

Figure 9. Comparison between the volume grain size (minor axis) of the sediment (curve) and both specimens of *Difflugia oblonga* (histograms). The lines designed by α and β are indicating the equivalent size of pseudostomes of specimens 1 and 2, respectively.

such environments, and their origin might be linked to infilling of the Flemish maritime plain (Gandouin et al., 2005) with minerals inherited from the Cotentin outcrops (Goguel & Graindor, 1963; Graindor & Payreyn, 1969) and vectored by marine currents during the Holocene. This observation opens the way to additional work on grain tracing and mineral fluxes from sources to basin deposits using observations on protist tests.

Contribution of Physico-Chemical Techniques to the Test Characterization

The first techniques used for surface testate amebae analysis were field cell-chemistry and chromatography for organic investigation (e.g., Moraczewski, 1971). The results were focused on the determination of the organic structure of the test. The mineral analysis came as a second step, by acid attack of the test and analyses of the residuals. Using these techniques, Saucin-Meulenberg et al. (1973) determined the occurrence of silicic material in *Arcella* spp., *Arcella hemisphaerica*, *Difflugia acuminata*, *Pontigulasia bigibbosa* tests, and in *Plagiopyxis callida*, and *Plagiopyxis declivis* with the additional use of RX-spectrography. Stout and Walker (1976) observed the surface of *Difflugia*, *Centropyxis*, *Cyclopyxis*, and *Euglypha* with an X-ray micro-analyzer. They distinguished between major constituents (mostly Si, and Al only in the case of *Difflugia*), significant constituents (Al, K, and Ca), and trace constituents (Na, Cl, Ca, and Al).

The use of SEM coupled with EDS allowed for both determination of grain shape and atomic composition. EDS was first used by Yamaoka and Mizuhira (1987) for analyzing the elemental composition of the scales in *Cochliopodium* spp., which are idiosomes of calcium. The cell investigation allowed for determination of the implication of Golgi vesicules for the calcium combination of scale construction. Then, Ogden (1988) used the same technique to analyze the organic structure of some *Difflugia* spp. that were able to build their test in the absence of available minerals within their surroundings. The author observed the occurrence of Ca, Mg, Fe, and P. The same technique was extensively used by Armynot du Châtelet et al. (2010) who used elemental analysis to determine the mineral composition and finally showed that mineral composition of the testate amebae depends on the environment and not on the species. In our study, the testate amebae tests were composed exclusively of major elements (Al, Ca, Fe, K, Mg, Na, and Si). No trace elements were observed. This is most probably linked to chemical elements available in the surrounding grains.

Surface and Structure of the Test

We observed that the skeleton of the analyzed specimens is not randomly built but presents a certain spatial organization, including grain size selection and grain orientation. These results are similar to those observed in other species such as *D. lobostoma* (Eckert & McGee-Russell, 1974). In that case, the authors established, after acid treatment and further observations, that the test was made of a single layer of grains that could be totally or sometimes partially dissolved by hydrofluoric acid.

We observed that the specimens selected only the smallest grains to form their test. Eckert and McGee-Russell (1974) had already observed that sand grains used in test construction were apparently picked according to their size and placed on specific locations. No apparent relationship, however, seems to exist between the size of the test and the size of the selected grains. During test construction, both large and small grains must be continually stored and placed on the test according to their size to form the complex pattern. Nevertheless, the maximum size of the incorporated grains seems limited by the size of the pseudostome.

The precise quantification of the rate of growth during cell division can be done through XMT observation. This can be used for evaluation of a soil ecosystem biomass of which testate amebae are an important component (Foissner, 1987, 1999; Aoki et al., 2007). For example, Netzel (1972) observed division of the cell of *Difflugia oviformis*. In a following study Netzel (1979) explained that during the division, the daughter cell could increase its size by a factor up to 2. 3D characterization could improve the results of this study by estimating the exact volume of the specimens from which their weight and biomass can then be deduced.

Ogden and Fairman (1979) highlighted that difficulties are often encountered with attempting to identify speci-

mens of testate amebae belonging to the genus *Difflugia* (the problem is still not solved). He gave some measurements of different specimens. When comparing our results to the *Difflugia oblonga* specimens he measured, our specimens are by far the biggest. Nevertheless, he concluded that a relationship exists between the size of the aperture and the test length. This ratio is very similar to what could be calculated for our specimens by taking into account the standard deviation: the present breadth/length is 0.48 ± 0.02 whereas it was 0.45 ± 0.04 for Ogden and Fairman (1979) specimens, and the diameter of the aperture/length is 0.18 ± 0.02, whereas it was 0.15 ± 0.02 for Ogden and Fairman (1979) specimens. Considering that this argument confirms that our specimens are *D. oblonga*, one wonders what may be the size of the largest possible specimen.

Conclusion

The developed techniques of ESEM-EDS, micro-probe analysis, CL, and XMT have allowed determination of the minerals, nature, quality, shape, volume, and architecture of the test of four specimens of *D. oblonga*. Determination of the mineralogy of the grains forming the test allowed for the determination of the degree to which the ameba selects the minerals. This new approach opens up new routes toward studies on mineral fluxes transported through water or air, ecological, and taxonomical studies. The observed minerals were shown to be inherited from local and distant outcrops.

D. oblonga agglutinates grains selected among the low size fraction of the available surrounding sediment. The size appears to be limited by the size of the pseudostome. The selected grains are oriented preferentially along their long axis, wrapping around the cell. Close to the pseudostome, the volume range of the grains is the smallest. Small grains are also found in the whole structure of the testate, where they fit in between bigger grains. It will be interesting to compare these patterns with those of other agglutinated species of genus *Difflugia* as well as other shelled protozoa.

XMT is useful for precise determination of the test structure and architecture. These measurements are helpful for characterizing the test—taxonomy—and evaluating the biomass. The approach broadens the understanding of testate amebae shell morphology and should be useful for further studies.

Acknowledgments

Dominique Bernard (Institut de Chimie de la Matière Condensée de Bordeaux) is sincerely acknowledged for having acquired the test images at the Swiss Light Source. Alissa MacMillan is gratefully acknowledged for her very careful reading of the paper. Philippe Recourt (Université Lille 1) is acknowledged for help with sampling in the Clairmarais pond and ESEM-EDS acquisition, and Jean-Luc Potdevin (Université Lille 1) for fruitful discussion about silicate minerals. The helpful comments and suggestions of Edward Mitchell and an anonymous reviewer are also gratefully acknowledged.

References

Aoki, Y., Hoshino, M. & Matsubara, T. (2007). Silica and testate amoebae in a soil under pine-oak forest. *Geoderma* **142**(1–2), 29–35.

Armbruster, T., Bonazzi, P., Akasaka, M., Bermanec, V., Chopin, C., Gieré, R., Heuss-Aassbichler, S., Liebscher, A., Menchetti, S., Pan, Y. & Pasero, M. (2006). Recommended nomenclature of epidote-group minerals. *Eur J Mineralogy* **18**, 551–567.

Armynot du Châtelet, E., Guillot, F., Recourt, P., Ventalon, S. & Tribovillard, N. (2010). Influence of sediment grain size and mineralogy on testate amoebae test construction. *Comptes Rendus Geoscience* **342**, 710–717.

Bernard, D. & Chirazi, A. (2006). Numerically enhanced microtomographic imaging method using a novel ring artefact filter. In *Advances in X-Ray Tomography for Geomaterials*, Desrues, J., Viggiani, G. & Bésuelle, P. (Eds.), p. 452. London: ISTE.

Charman, D.J. (2001). Biostratigraphic and palaeoenvironmental applications of testate amoebae. *Quaternary Sci Rev* **20**(16–17), 1753–1764.

Drever, J.I. (Ed.) (1985). *The Chemistry of Weathering*. New York: Reidel.

Eckert, B.S. & McGee-Russell, S.M. (1974). Shell structure in *Difflugia lobostoma* observed by scanning and transmission electron microscopy. *Tissue Cell* **6**(2), 215–221.

Foissner, W. (1987). Soil protozoa: Fundamental problems, ecological significance, adaptations in ciliates and testaceans, bioindicators, and guide to the literature. *Prog Protistology* **2**, 69–212.

Foissner, W. (1999). Soil protozoa as bioindicators: Pros and cons, methods, diversity, representative examples. *Agr, Ecosyst Environ* **74**, 95–112.

Gandouin, E., Franquet, E. & Van Vliet-Lanoë, B. (2005). Chironomids (Diptera) in river floodplains: Their status and potential use for palaeoenvironmental reconstruction purposes. *Archiv für Hydrobiologie* **162**(4), 511–534.

Gilbert, D., Amblard, C., Bourdier, G., Francez, A.-J. & Mitchell, E.A.D. (2000). Le régime alimentaire des Thécamoebiens (Protista, Sarcodina). *Année Biologique* **39**, 57–68.

Goguel, J. & Graindor, M.-J. (1963). *Cartes géologiques de la France au 1/50 000- Feuille de Cherbourg*. Orléans, France: BRGM.

Gonzales, R.C. & Woods, R.E. (1992). *Digital Image Processing*. Reading, MA: Addison-Wesley Publishing Company.

Graindor, M.J. & Payreyn, C. (1969). *Cartes géologiques de la France au 1/50 000- Feuille de Saint-Vaast-la-Hougue*. Orléans, France: BRGM.

Hawthorne, F.C. & Oberti, R. (2007). Classification of the amphiboles. *Rev Mineral Geochem* **67**, 55–88.

Herman, G.T. (1980). *Image Reconstruction from Projections: Fundamentals of Computerized Tomography*. New York: Academic Press.

Loizeau, J.-L., Arbouille, D., Santiago, S. & Vernet, J.-P. (1994). Evaluation of a wide range laser diffraction grain size analyser for use with sediments. *Sedimentology* **41**, 353–361.

McCave, I.N., Manighetti, B. & Robinson, S.G. (1995). Sortable silt and fine sediment size/composition slicing: Parameters for palaeocurrent speed and palaeoceanography. *Paleoceanography* **10**(3), 593–610.

Moraczewski, J. (1971). La composition chimique de la coque d'Arcella discoides Ehrbg. *Acta Protozoologica* **8**, 423–437.

Netzel, H. (1972). Die Schalenbildung bei Difflugia oviformis (Rhizopoda, Testacea). *Zoologisches Zellforsch* **135**, 55–61.

Netzel, H. (1979). Morphogenesis in testaceous amoebae. *Eur J Cell Biol* **20**, 116–135.

Ogden, C.G. (1988). Morphology of the organic shell matrix of *Difflugia* (Rhizopoda) in culture, inclusing modification by the addition of agglutinate particles. *Archiv für Protistenkunde* **136**, 365–376.

Ogden, C.G. & Fairman, S. (1979). Further observations on pyriform species of *Difflugia* (Rhizopodea). *Archiv für Protistenkunde* **122**, 372–381.

Patterson, T. & Kumar, A. (2000). Use of Arcellacea (Thecamoebians) to gauge levels of contamination and remediation in industrially polluted lakes. In *Environmental Micropaleontology*, Martin, R.E. (Ed.), pp. 257–278. New York: Kluwer Academic/Plenum.

Reinhardt, E.G., Dalby, A.P., Kumar, A. & Patterson, T. (1998). Arcellaceans as pollution indicators in mine tailling contaminatings lakes near Cobalt, Ontario, Canada. *Micropaleontology* **44**(2), 131–148.

Salvo, L., Cloetens, P., Maire, E., Zabler, S., Blandin, J.J., Buffière, J.Y., Ludwig, W., Boller, E., Bellet, D. & Josserond, C. (2003). X-ray micro-tomography an attractive characterisation technique in materials science. *Nucl Instrum Methods Phys Res B* **200**, 273–286.

Saucin-Meulenberg, M., Bussers, J.C. & Jeuniaux, C. (1973). Composition chimique de la thèque de quelques thécamoebiens (Protozoaires). *Bulletin Biologique de la France et de la Belgique* **107**, 107–113.

Scott, D.B., Medioli, F.S. & Schafer, C.T. (2001). *Monitoring in Coastal Environments Using Foraminifera and Thecamoebian Indicators*. New York: Cambridge University Press.

Stout, J.D. & Walker, G.D. (1976). Discrimination of mineral particles in test formation by thecamoebae. *Trans Am Microsc Soc* **95**(3), 486–489.

Trentesaux, A., Recourt, P., Bout-Roumazeilles, V. & Tribovillard, N. (2001). Carbonate grain-size distribution in hemipelagic sediments from a laser particle sizer. *J Sediment Res* **71**(5), 858–862.

Waterlot, G. (1968). *Cartes géologiques de la France au 1/50 000—Feuille de Cassel*. Orléans, France: BRGM.

Yamaoka, I. & Mizuhira, V. (1987). X-ray microanalysis of the mineral components in the scales of an amoeba, Cochliopodium sp. (Testacea). *Cell Tissue Res* **247**, 633–637.